Systematic Structure in the *K*-Edge Photoabsorption Spectra of the 4*d* Transition Metals: Theory

J. E. Muller[a] and O. Jepsen
Nordita, DK-2100 Copenhagen, Denmark

and

O. K. Andersen
Department of Electrophysics, Technical University, DK-2800 Lyngby, Denmark

and

J. W. Wilkins
Materials Science Center, Cornell University, Ithaca, New York 14853
(Received 8 December 1977)

The *K*-edge photoabsorption spectra of the 4*d* metals calculated by the linear augmented-plane-wave method yield good agreement with the measured data. The prominent systematic features of the spectra, most easily discussed in terms of the $l = 1$ projected density of final states, are simply related to the underlying band structure. The results for Zr, Mo, Pd, and Ag are presented here.

We present the first systematic calculation of the *K*-edge photoabsorption spectra of the 4*d* transition metals and find that all the major features in the calculated and measured[1] spectra can be directly related to strong features in the $l = 1$ projected density of final states. These features can be simply explained in terms of elementary aspects of the underlying band structure, which we have computed by the linear augmented-plane-wave method.[2]

The organization of this Letter is as follows: First we compare the results of our calculation of the photoabsorption spectra with the experimental curves to focus on certain common systematic features. Then we demonstrate that all these features are present in the $l = 1$ projected density of band states $N_1(E)$. Finally the physical origin of these features is explained and their systematic behavior across the 4*d* row is discussed.

The calculated and measured *K*-edge absorption spectra are presented in Fig. 1(a) for metals which span the 4*d* row and its assorted crystal structures; i.e., hcp Zr, bcc Mo, fcc Pd, and fcc Ag.

Several clear features are present both in the experimental data and in our calculations: (1) three peaks (or, more precisely, regions of increased absorption) named *d*, *p*, and *f* which will be identified with peaks in the density of final states having 4*d*-, 5*p*-, and 4*f*-orbital character; (2) two valleys (or, more precisely, regions of decreased absorption) between the above-mentioned peaks which will be identified with valleys in the density of final states caused by hybridization of the 5*p* orbitals with the 4*d* and 4*f* orbitals.

Within the dipole approximation the *K*-edge absorption coefficient for a photon of energy E ejecting an electron from a 1*s* state (with energy E_{1s}) to an empty conduction-band state (with energy $E_{\vec{k},n}$) is proportional to

$$\mu(E) \propto \sum_{\vec{k},n} |\langle \psi_{1s} | \vec{r} | \psi_{\vec{k},n} \rangle|^2 \times \delta(E - E_{\vec{k},n} + E_{1s}), \quad (1)$$

where we note that $E_{\vec{k},n}$ must be above the Fermi level for any transition to occur. In Fig. 2 we show $\mu(E)$ for Pd. Two additional considerations were required in order to make the comparison with the experiments shown in Fig. 1(a): (1) $\mu(E)$ was convoluted with a Lorentzian whose width included the width of the 1*s* hole[3] (3–7 eV) and the width of the conduction-electron final state due to electron-electron scattering[4] (~1 eV). (2) To include the effects of instrumental resolution, the result of (1) was convoluted with an appropriate window function which produced an additional smearing of roughly 1 eV. The resulting curves are shown in Fig. 1(a), and we notice that with the assumptions in Eq. (1) we have reproduced all the observed fine structure of the spectra up to about 50 eV above the Fermi level.

We observe that $\langle \psi_{1s} | \vec{r}$ in $\mu(E)$ acts as an operator which projects out the $l = 1$ part of the conduction bands. Accordingly, we define the $l = 1$ projection, into the muffin-tin sphere[2] of the ex-

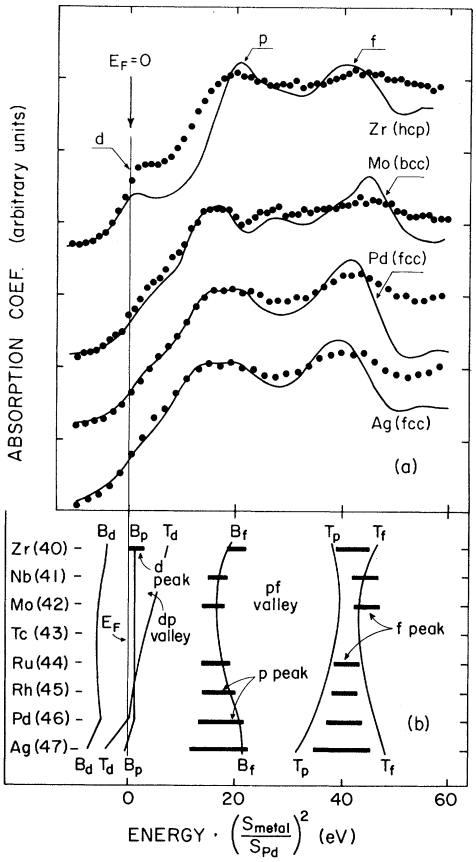

FIG. 1. (a) Calculated (solid lines) and measured (dotted lines) K-edge adsorption spectra for some of the $4d$ transition metals. The complete "three peak" structure is most clearly seen in Zr: The peaks named d, p, and f arise from states having $4d$-, $5p$-, and $4f$-orbital character, respectively. (b) Systematic features of the spectra across the $4d$ row. The bottom (B_l) and the top (T_l) of the individual nl bands, as given by the Wigner-Seitz rules, are shown in solid lines. The positions of the d, p, and f peaks are indicated by the horizontal bars. Also the positions of the hybridization valleys dp and pf are shown. The common abscissa is $(E-E_F)(S/S_{Pd})^2$, where S is the radius of the Wigner-Seitz sphere. This scaling removes the atomic-volume dependence due to the largely kinetic (free-electron) character of the energy.

cited atom,[5] of the density of states as

$$N_1(E) = \sum_{\vec{k},n} \sum_{m_l} |\langle l=1, m_l | \psi_{\vec{k},n} \rangle_{MT}|^2 \times \delta(E - E_{\vec{k},n}) . \quad (2)$$

The ratio $\mu(E)/N_1(E)$, shown in Fig. 2, demonstrates that for $E > E_F$ all the structure of $\mu(E)$ is retained in $N_1(E)$ which we next consider (Fig. 3).

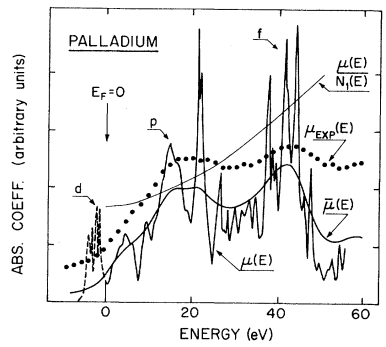

FIG. 2. The calculated absorption coefficient for Pd before [$\mu(E)$] and after [$\bar{\mu}(E)$] it has been smeared out to account for lifetime effects and for instrumental resolution. The curve $\mu(E)/N_1(E)$ demonstrates that all the fine structure of $\mu(E)$ is contained in $N_1(E)$. The experimental data $\mu_{EXP}(E)$ has been included for comparison.

The underlying band structure is most conveniently described in terms of nl bands constructed from linear combinations of nl orbitals[6] and, in Fig. 3, we show the densities of states for the individual $4d$, $5p$, and $4f$ bands[7] together with $N_1(E)$. The shape of $N_1(E)$ may be explained as follows: (1) Neglecting hybridization between the

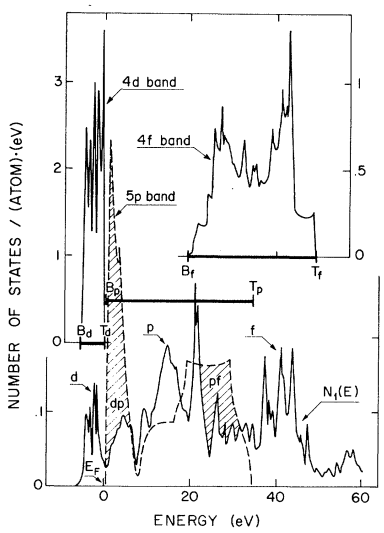

FIG. 3. The $l = 1$ projected density of states $N_1(E)$ and the densities of states for the $4d$, $5p$, and $4f$ bands of Pd. For comparison with the nl bands, $N_1(E)$ has been multiplied by the ratio of the volumes of the Wigner-Seitz and the muffin-tin spheres. The shaded areas indicate the suppressions which produce the dp and pf valleys. The horizontal bars indicate the width of the individual nl bands as given by the Wigner-Seitz rules.

nl bands, we find that the $5p$ band, being derived from orbitals with $l=1$, contributes directly to $N_1(E)$ and that the $4d$ and $4f$ bands contribute via the $l=1$ projection of the tails of the $4d$ and $4f$ orbitals centered at sites adjacent to the excited atom. (2) With the inclusion of hybridization $N_1(E)$ is depressed in those regions where the nl bands overlap and it is enhanced in the adjacent regions.

In Fig. 3, therefore, the central peak labeled p arises from the $5p$ band and the peaks labeled d and f are replicas of those parts of the $4d$ and $4f$ bands which do not overlap the $5p$ band. The valleys labeled dp and pf are due to hybridization and they occur where the $4d$ and $4f$ bands overlap the $5p$ band.[8]

The widths and locations of the nl bands are determined by the crystal potential,[9] and we observe that the extrema of nl bands agree well with the positions B_l (bottom) and T_l (top) obtained from the simple Wigner-Seitz rules[10] and indicated in Fig. 3. The major peaks and valleys in the absorption spectrum will therefore be positioned as follows: peak d in the region (E_F, B_p), valley dp in the region (B_p, T_d), peak p in the region (T_d, B_f), valley pf in the region (B_f, T_p), and peak f in the region (T_p, T_f).[11]

The systematic behavior of the major peaks and valleys in the absorption spectra shown in Fig. 1(a) follows from the position of the Fermi level and the Wigner-Seitz rules. This is demonstrated in Fig. 1(b). As the $4d$ band is filled, peak d disappears and peak p widens because the top of the $4d$ band falls in energy.

Finally, we note that the strong features of the spectra are essentially determined by the underlying potential. As a result, the major peaks and valleys (a) show a simple systematic behavior across the $4d$ row, (b) can be located in energy without need of a band-structure calculation (i.e., by using the Wigner-Seitz rules), and (c) do not depend on the crystal structure.[12]

This work was supported in part by the Materials Science Center under a grant from the National Science Foundation.

---

[a]Present address: Department of Physics, and Materials Science Center, Cornell University, Ithaca, N. Y. 14853. Permanent address: Facultad de Ciencias Física y Matemáticas, Universidad de Chile, Santiago, Chile.

[1]V. O. Kostroun, R. W. Fairchild, C. A. Kukkonen, and J. W. Wilkins, Phys. Rev. B 13, 3268 (1976).

[2]O. Krogh Andersen, Phys. Rev. B 12, 3060 (1975). For each metal the total energy range of approximately 50 eV was divided into three energy panels (for Pd, $E_v = 5.4$, 24, and 43 eV) and a linear augmented-plane-wave calculation was carried out in each of these. The standard muffin-tin potential, constructed according to the Mattheiss prescription, was used. The relativistic shifts were included but the spin-orbit coupling was neglected.

[3]For atomic number $Z > 40$, the width of the $1s$ core hole is given by $1.73Z^{3.93} \times (10^{-6}$ eV). See H. J. Leisi *et al.*, Helv. Phys. Acta 34, 16 (1961).

[4]I. Lindau and W. E. Spicer, J. Electron Spectrosc. 3, 409 (1974). Although the width probably increases with energy in the energy range of interest, we have chosen it to be a constant for convenience. Moreover, at higher energies, where the band effects are smaller, one should first take the mean free path into account and hence derive the conventional extended–x-ray–adsorption fine-structure formula. See, for example, C. A. Ashley and S. Doniach, Phys. Rev. B 11, 1297 (1974).

[5]Note that this is strictly a one-electron calculation. Any distortion of the edge due to many-body effects would presumably be smaller than the smearing of the edge. See also Refs. 1 and 3.

[6]For the nl bands we used the canonical bands defined in Ref. 2. See also O. K. Andersen and O. Jepsen, Physica (Utrecht) 91 B, 317 (1977).

[7]The $5s$ and $5d$ bands do not enter our simplified discussion because their densities of states are small in the energy region of interest.

[8]For Pd the $4d$ and $4f$ bands do not overlap, but do hybridize. The dp valley is seen clearly in the first part of the $4d$ row; see Fig. 1(b).

[9]The crystal structure is reflected in the shapes of the nl bands and hence in the detailed structure of $N_1(E)$ and $\mu(E)$.

[10]The Wigner-Seitz rules state that the bottom B_l and the top T_l of the nl band are approximately given by $\varphi_l'(B_l, S) = 0$ and $\varphi_l(T_l, S) = 0$, where $\varphi_l(E, r)$ is the radial part of the wave function of energy E, and S is the radius of the Wigner-Seitz sphere.

[11]In a monovalent, free-electron metal the Wigner-Seitz band extrema are $(B_s, T_s) = (-6.1, 10.2)$, $(B_p, T_p) = (0.95, 27.2)$, $(B_d, T_d) = (12.4, 48.7)$, and $(B_f, T_f) = (27.4, 74.4)$ eV, using the same energy scale as in Figs. 1–3. In this case $N_1(E)$ and $\mu(E)$ exhibit one broad peak centered at 10.2 eV. By comparison, the "three-peak" structure found in the $4d$ metals is caused by the presence of the $4d$ band and by the $4f$ band being relatively narrow and low lying.

[12]The crystal structure, which enters in the shape of the individual nl bands, gives rise after hybridization to much weaker features. However, in some cases, signatures of the crystal structure can be seen in the spectra. For instance, the small bump between the p and f peaks in the spectrum of molybdenum is due to a peak present in the $l = 1$ band only for the bcc lattice.